Journal Pre-proofs

Full Length Article

Assembly of N- and P-functionalized carbon nanostructures derived from precursor-defined ternary copolymers for high-capacity lithium-ion batteries

Luyao Guo, Mengru Wang, Ronghe Lin, Jiaxin Ma, Shuanghao Zheng, Xiaoling Mou, Jun Zhang, Zhong-Shuai Wu, Yunjie Ding

PII: S1004-9541(22)00149-5
DOI: https://doi.org/10.1016/j.cjche.2022.01.032
Reference: CJCHE 2624

To appear in: *Chinese Journal of Chemical Engineering*

Received Date: 15 October 2021
Revised Date: 5 January 2022
Accepted Date: 10 January 2022

Please cite this article as: L. Guo, M. Wang, R. Lin, J. Ma, S. Zheng, X. Mou, J. Zhang, Z-S. Wu, Y. Ding, Assembly of N- and P-functionalized carbon nanostructures derived from precursor-defined ternary copolymers for high-capacity lithium-ion batteries, *Chinese Journal of Chemical Engineering* (2022), doi: https://doi.org/10.1016/j.cjche.2022.01.032

Article

Assembly of N- and P-functionalized carbon nanostructures derived from precursor-defined ternary copolymers for high-capacity lithium-ion batteries

Luyao Guo[1], Mengru Wang[1], Ronghe Lin[1,*], Jiaxin Ma[2,3], Shuanghao Zheng[2,5], Xiaoling Mou[1], Jun Zhang[4,*], Zhong-Shuai Wu[2,5], Yunjie Ding[1,2,5,*]

[1]Hangzhou Institute of Advanced Studies, Zhejiang Normal University, Hangzhou 311231, China

[2]State Key Laboratory of Catalysis, Dalian Institute of Chemical Physics, Chinese Academy of Sciences, Dalian 116023, China

[3]University of Chinese Academy of Sciences Yuquan Road 19A, Shijingshan District, Beijing 100049, China

[4]College of Chemistry, Chemical Engineering and Materials Science, Soochow University, Suzhou 215123, China

[5]Dalian National Laboratory for Clean Energy, Dalian Institute of Chemical Physics, Chinese Academy of Sciences, Zhongshan Road 457, 116023 Dalian, China

* Corresponding authors. Emails: catalysis.lin@zjnu.edu.cn; jzhang2017@@suda.edu.cn; dyj@dicp.ac.cn. Tel/Fax: +86 571 84379057.

[+]Equal contribution.

Abstract: Synthesis of new carbon nanostructures with tunable properties is vital for precisely regulating electrochemical performance in the wide applications. Herein, we report a novel approach for the oxidative polymerization of N- and P-bearing copolymers from the self-assembly of three different monomers (aniline, pyrrole, and phytic acid), and further prepare the respective carbon nanostructures with relatively consistent N dopant (6.2%−8.0%, atom) and varying P concentrations (0.4%−2.8%, atom) *via* controllable pyrolysis. The impacts of phytic acid addition on the compositional, structural, and morphological evolution of the copolymers and the resulting nanocarbons are well studied through a spectrum of characterizations including N_2 sorption, Fourier transform infrared spectroscopy, gel permeation chromatograph, scanning/transmission electron microscopy, and X-ray photoelectron spectroscopy. Gradual fragmentation of the nanosphere structures is evidenced with increasing addition of phytic acid, leading to different nanostructures from hollow nanospheres to 3D aggregates. Nanocarbons decorated with N and P dopants from pyrolysis are further utilized as anode materials in lithium-ion batteries, demonstrating enhanced electrochemical performance, *i.e.*, a reversible capacity of 380 $mA{\cdot}h{\cdot}g^{-1}$ at 2 $A{\cdot}g^{-1}$ for NPC-0.5 during 200 cycles. The superior performance originates from the balanced porosity, and appropriate concentrations of P and pyrrolic N, thus pointing the direction for designing high-performance anode materials.

Keywords: Carbon nanospheres, Doping, Lithium-ion batteries, Polymers, Porosity.

1. Introduction

Metal-free nanocarbon materials are raising as a family of fascinating advanced functional materials with wide applications in many fields, such as battery, supercapacitor, adsorbent, and thermal- and electro-catalysis [1-9]. Doping foreign atoms such as p-block elements (N and P) into the carbon frameworks, which can induce the re-distribution of local electrons around newly created defects[10], has been demonstrated as an effective strategy to significantly improve their performance. While N-doped carbons are the most studied materials, increasing attentions have recently been paid to N- and P-co-doped carbons (NPCs) nanostructures with unique characters due to the incorporation of P with a larger radius. In this aspect, the applications of different NPCs structures have been greatly explored in electro-catalysis[11-17], photo-catalysis,[18] supercapacitors[12, 19], batteries[20], photoluminescence [21] and cellular imaging [22], *etc*. While the boosted performance was usually ascribed to the increased number of defective sites, for example, different nitrogen species like pyridinic, pyrrolic, and graphitic N were the typically speculated active sites [23-25], the porosity of the hosts might also be altered upon doping and thus played a role in determining the performance. This calls for a closer examination on their performance by considering both the compositional and structural properties.

Among the reported approaches for NPC synthesis, the pyrolysis of N- and/or P- bearing polymers or ionic liquids, with or without the participation of additional phosphorous source, is an effective strategy. For instance, Yang *et al*. prepared highly porous NPCs (specific surface area S_{BET}=1535 $m^2 \cdot g^{-1}$) through the pyrolysis of imine-linked porous organic polymers bearing both the N- and P-containing functional groups.[26] Xia *et al*. synthesized NPCs with a nanosheet morphology *via* pyrolyzing [Hvim]DHP, an ionic liquid derived from H_3PO_4 functionalized vinyl imidazole[27]. Further, the sheet-like NPCs were also synthesized by direct carbonization of graphene with P-containing ionic liquid-MBMG-PF_6 [15]. He *et al*. reported a novel method to fabricate NPCs microspheres by hydrothermally treating carbon microspheres with $(NH_4)_2HPO_4$, followed by

pyrolyzing the obtained assembles[19]. NPCs can also be prepared by the direct carbonization of P-containing copolymers from the assembly of different monomers[14]. In this context, phytic acid was the monomer of choice selected as the phosphorous source to complex with other monomers such as aniline[14, 28, 29] and pyrrole[16], or with gelatin[30] to yield supramolecular assemblies. Pyrolyzing treatment, sometimes in conjunction with chemical activation, can bring ultra-high S_{BET} and rich porosity to the 3D NPC foams, leading to excellent performance in the oxygen reduction/evolution reactions[29], supercapacitors and lithium-sulfur batteries[28].

The previous synthesis of NPCs based on the copolymerization of different monomers mainly adopted phytic acid-containing binary monomer systems. However, systematic regulation of the composition, structure, and morphology of the copolymer precursors and the corresponding NPCs has been scarcely conducted. In the seminal work by Guo and co-workers[31], a template-assisted fabrication of aniline-pyrrole copolymers with a hollow nanosphere morphology was proposed. Hollow NPC nanospheres were yielded after subsequent pyrolysis, clearly showing a memory effect[32, 33]. Notably, this morphology differs greatly with those of the phytic acid-aniline or phytic acid-pyrrole analogues typically exhibiting a 3D aggregate structure[28, 29, 32]. In this work, the template-assisted assembly of phytic acid-aniline-pyrrole ternary systems was studied. The selection of this targeted system was beneficial to discriminate the effect of phytic acid incorporation on the morphological evolution of the resultant copolymers. By varying the concentration of phytic acid in the initial polymerization solutions, we systematically studied the different properties of the copolymers and the respective NPCs by applying combined characterization techniques. Hollow NPC nanospheres were obtained by carefully tuning the addition of phytic acid, and these well-defined nanostructures gradually fragmented and changed to conventional aggregates at higher P doping levels accompanied with the compromised porosity. The array of NPC nanostructures was adopted as anodes in lithium-ion batteries, and the electrochemical performance in relation to the different speciation (N and P) and porosity were

discussed.

2. Experimental

2.1. Materials synthesis

The aniline-pyrrole-phytic acid copolymer (denoted as PAniPyPA) was synthesized by a previously established protocol [31] with a few modifications. A mixture of TX-100 (1.6 mmol, Aladdin, BR), aniline (50 mmol, Acros, 99.5%), pyrrole (50 mmol, Sigma-Aldrich, 98%), and different amount of phytic acid (Aladdin, 70% in H_2O) was dissolved in 160 cm^3 deionized water, and stirred at 500 rpm at room temperature until a homogeneous solution was obtained. The solution was then stored in fridge (278 K) for 30 min before use. Another solution of ammonium persulfate (4.56 g, Acros Organics, 98%, dissolved in 40 cm^3 deionized water) was prepared, cooled at ice bath for 30 min, and then added in one portion into the above monomer-containing solution with vigorous stirring at room temperature. Afterwards, the polymerization was continued for overnight. The yielded solids were filtrated, washed with deionized water, immersed in deionized water for two days, and freeze-dried for 24 h to produce dry aerogel. The as-prepared copolymers were further converted to corresponding N- and P-doped carbons in a tubular oven by pyrolysis in flowing N_2 at 1073 K (5 $K \cdot min^{-1}$, 5 h). These copolymer assemblies and the corresponding nanocarbons were coined as PAniPyPA-*x* and NPC-*x*, where *x* (*x*=0.1, 0.2, 0.5, and 1.0) denotes the calculated molar P:N ratio in the added monomers. A phosphorous-free aniline-pyrrole copolymer and the corresponding nanocarbons, denoted as PAniPy and NC, respectively, were also synthesized for comparison purpose by following the similar procedures as mentioned above but without the addition of phytic acid.

2.2. Characterizations

N_2-sorption isotherms were recorded at 77 K on a Micromeritics ASAP 2010 instrument. Before the measurement, the sample was degassed at 573 K for 6 h. The specific surface area (S_{BET}) was calculated by the Brunauer-Emmett-Teller (BET) method using the adsorption branch. IR spectra were recorded on a Bruker vector-22 FTIR spectrometer. A self-supported wafer with a diameter of 1.2 cm was prepared by pressing a powder mixture (10 mg) containing 5% sample and 95% KBr and then mounted into the IR cell. The Fourier transform infrared spectroscopy (FTIR) measurement was operated in the absorbance mode and the spectra were collected in the region of 4000−400 cm^{-1} using a resolution of 4 cm^{-1} and 32 scans. The spectrum of the KBr recorded at room temperature was taken as the background. The average molecular weight of selected copolymers was measured with an Agilent 1100 GPC equipped with two PFG linear M columns, connected in series with an Agilent 1100 DIR detector. The samples were eluted in hexafluoroisopropanol with 0.02 M potassium trifluoroacetate at 1 cm^3 min^{-1} at room temperature. Calibration of the GPC spectra was conducted with the polystyrene standards. Scanning electron microscopy (SEM) was conducted on a Quanta 200F instrument operating at 10 kV and 50 pA. The powder sample was dispersed in dry form onto fresh carbon paint deposited on an aluminum holder and subsequently coated by a Pt-Pd alloy (ca. 10 nm thickness) to prevent charging. Transmission electron microscopy (TEM) images were taken on a Philips FEI Tecnai G^2 microscopy operating at 120 kV. The specimen was prepared by ultrasonically dispersing the powder sample in ethanol, depositing droplets of the suspensions onto carbon-coated copper or gold grids, and drying in air. X-ray photoelectron spectroscopy (XPS) was measured in a Physical Electronics Quantum 2000 X-ray photoelectron spectrometer using monochromatic Al-K□ radiation, generated from an electron beam operated at 15 kV, and equipped with a hemispherical capacitor electron-energy analyzer. The solids were analyzed at the electron take-off angle of 45° and the pass energy of 46.95 eV. The spectrometer was calibrated for the Au $4f_{7/2}$ signal to be at 84.0±0.1 eV and had a

resolution step width of 0.2 eV. Charge compensation was applied by shifting the C 1*s* peaks to 285.0 eV. The N 1*s* envelopes were fitted by mixed Gaussian-Lorentzian component profiles after Shirley background subtraction. The selected peak positions of the different nitrogen species were based on literature reported data.[34] The elemental concentrations were quantified based on the measured photoelectron peak areas (C 1*s*, N 1*s*, O 1*s*, and P 2*p*) after Shirley background subtraction, using PHI-MultiPak software and the built-in relative sensitivity factors, which were corrected for the system transmission function. The electronic conductivity (*s*) of the samples were measured by the four-probe method (ST2742B). The powders were first pressed at different pressures before the data were collected.

2.3. Electrochemical test

Lithium ion batteries were assembled at CR2016 coin cells using lithium foil as the counter and reference electrode, NC and NPC-*x* electrodes as working electrodes, and 1.0 mol·L^{-1} solution of $LiPF_6$ in ethylene carbonate/dimethyl carbonate/diethyl carbonate (1:1:1) as electrolyte. The working electrodes were prepared through the mixture of N-doped carbon powder, carbon black, and polyvinylidene fluoride with a weight ratio of 8:1:1 in N-methylpyrrolidone solvent. The resultant electrode slurry was pasted onto a copper current collector, followed by vacuum drying at 393 K for 12 h, and then cut into electrode plate with a diameter of 12 mm. The galvanostatic charge-discharge (GCD) profiles were operated at a LAND CT2001A battery tester in a voltage range from 0.01 to 3.0 V. Electrochemical impedance spectroscopy (EIS) spectra and cyclic voltammetry (CV) curves were carried out at a CHI 760E workstation. The CV tests were conducted at 0.01-3.0 V with a scanning rate of 0.1 mV·s^{-1}. The EIS data were collected at an ac amplitude of 5 mV with the frequency range from 100000 to 0.1 Hz.

3. Results and Discussion

3.1. Synthesis and characterization of ternary copolymers

3.1.1. Compositional and structural properties

The self-assembly of aniline and pyrrole into carbon nanospheres in the presence of different surfactants has been documented previously[31-33]. Here we adopted TX-100 as the surfactant and introduced a third monomer-phytic acid with the aims to study the impact of phosphorous incorporation on the properties of as-derived N- and P-containing copolymers and to further obtain N- and P-doped nanocarbons with novel structures. For this purpose, a series of PAniPyPA copolymers was synthesized by controlling the addition of phytic acid at a fixed molar aniline: pyrrole ratio of 1.0. Four copolymers PAniPyPA-*x* (*x*=0.1, 0.2, 0.5, 1.0) were synthesized with the increasing addition of phytic acid, where *x* indicated the molar P:N ratio in the initial monomers (Fig. 1).

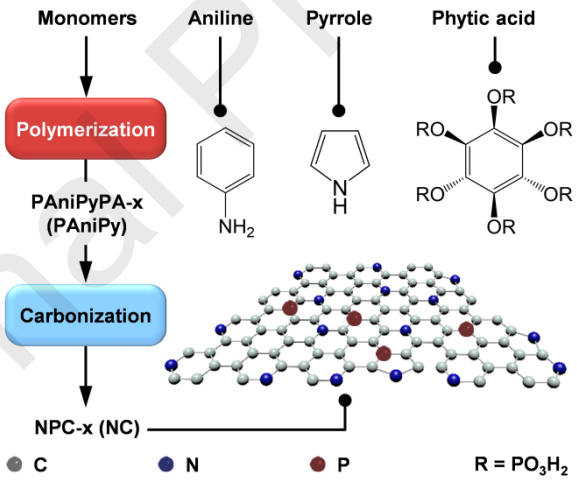

Fig.1. Synthetic strategy of the polyaniline-based polymers via oxidative polymerization of ternary monomers and the corresponding nanocarbon materials accompanied with the sample codes.

To study the addition of phytic acid addition on the polymerization process, the relative molecular weight (M_w) of selected polyaniline-based copolymers was examined by GPC analysis (Fig. 2(a)). Two peaks, typical for the polyaniline-based polymers[35], were observed at around 8 and 11.6 min

for PAniPy, PAniPyPA-0.1, and PAniPyPA-0.5. These can be assigned to the long-chained copolymers and the short-chained oligomers, respectively. The similar positions of the three samples likely suggested similar kinetics of the polymerization process. Indeed, the M_w and the shares of oligomers were 40787, 41958, and 42441 Daltons, and 34.5%, 30.9%, and 35.9%, respectively, for PAniPy, PAniPyPA-0.1, and PAniPyPA-0.5. The structures of these copolymers were then examined by FTIR (Fig. 2(b)). For PAniPy, several absorption bands were observed at 1493, 1450, 1110, 1048, 836, 759, 691, and 615 cm^{-1}. The bands at 1493 and 1110 cm^{-1} were assigned to the str*etc*hing vibrations related to the benzenoid and quinonoid rings, respectively; the band at 1450 cm^{-1} was related to the C═C str*etc*hing of aromatic ring; the additional bands at 836 and 759 cm^{-1} were due to the γ(C–H) vibrations in the 1,2,4-trisubstituted ring; and the bands at 1048 and 615 cm^{-1} were associated with the presence of sulfates (HSO_4^- and SO_4^{2-}) [36, 37]. These features were well inherited with the addition of small amounts of phytic acid at P:N = 0.2. However, the distinct bands related to polyanilines (1493 and 1110 cm^{-1}) disappeared at higher phosphorous doping levels (P:N > 0.5). Also, the intensities of the other bands for these two samples weakened greatly. These results suggested that the addition of phytic acid strongly disturbed the assembly of the copolymerization process. Noted that the vibrations of phosphates (878−1060 cm^{-1}) cannot be well visualized probably due to the overlapping with the other functional groups in the similar region. According to the study by Bao *et al*. [28], the negatively charged phosphate groups in the phytic acid molecules might interact with the positively charged amine groups in the backbone of the polyanilines through electrostatic attractions.

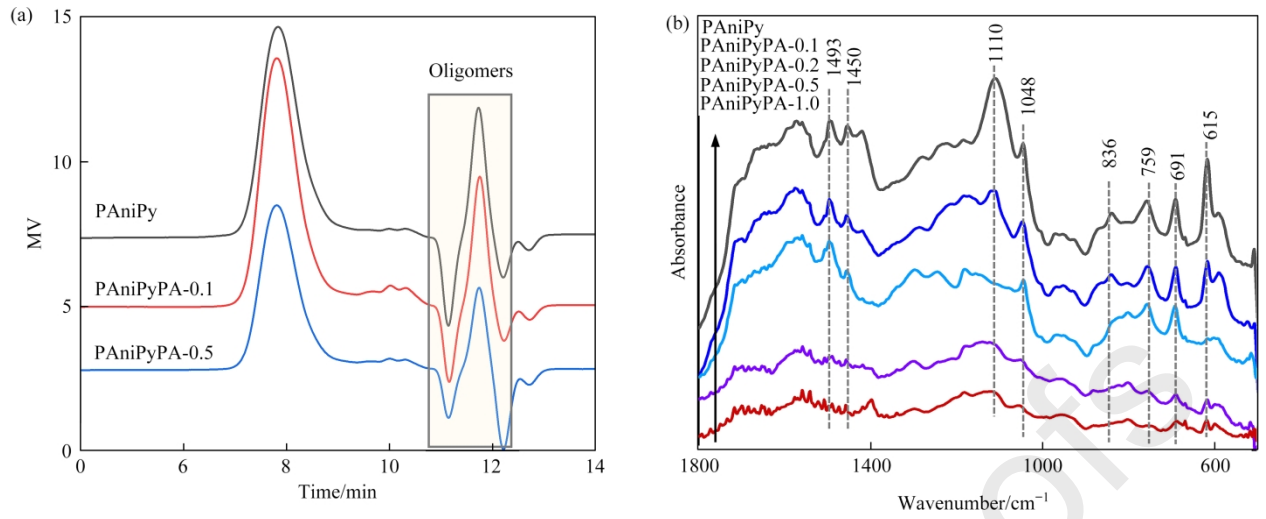

Fig. 2. (a) GPC profiles and (b) FTIR spectra of PAniPy and PAniPyPA-*x* samples.

3.1.2. XPS insights

The successful incorporation of phytic acid into the copolymer backbone was confirmed by XPS (Table 1). The atomic concentration of P increased steadily from 0.4% to 2.0% with the increasing *x* from 0.1 to 1.0. Meanwhile the N concentration stayed relatively at stable around 12%. In addition, the P:N ratios in the resulting copolymers were much lower than the set values, hinting that phytic acid was likely only partially incorporated during the polymerization process. Indeed, the P content and the P:N ratio almost leveled off at $x > 0.5$. Therefore, the copolymerization of the ternary systems, particularly the incorporation of phytic acid into the polymer backbone was likely self-limiting, restricting the higher doping of the phosphorous species. To probe the variation of nitrogen speciation upon adding phytic acid, the N1*s* XPS spectra of the different copolymers were further analyzed (Fig. 3(a), (b) and Table 1). Similar envelops at around 398-404 eV were observed for all the materials. A slight broadening of the peaks was evidenced for PAniPyPA-0.5 and PAniPyPA-1.0. Therefore, deconvolution of the spectra was conducted by fitting (Table S1). Three different speciation were found at the binding energies at *ca*. 399.7, 400.4, and 402.6 eV that were associated with amine (N2), oxidized amine ($N2^+$), and protonated imine ($N1^+$), respectively.[34]

Interestingly, the share of N2 species generally increased at the compensation of $N2^+$ with the increasing incorporation of phytic acid, indicating that the ternary copolymers were less oxidized than the binary analogue.

Table 1. The parameters of the polyamine-based polymers and the corresponding nanocarbons.

Sample[a]	V_{total}① /$cm^3 \cdot g^{-1}$	V_{micro}② /$cm^3 \cdot g^{-1}$	S_{meso}② /$m^2 \cdot g^{-1}$	S_{BET}③ /$m^2 \cdot g^{-1}$	r_P④ /nm	C⑤ /% (atom)	N⑤ /% (atom)	P⑤ /% (atom)	O⑤ /% (atom)	P:N⑤ /mol·mol^{-1}
PAniPy	—	—	—	—	—	66.2	13.2	0	20.6	0
PAniPyPA-0.1	—	—	—	—	—	67.5	12	0.4	20.1	0.033
PAniPyPA-0.2	—	—	—	—	—	70.5	12.6	1.1	15.8	0.087
PAniPyPA-0.5	—	—	—	—	—	63.4	10.5	1.9	24.2	0.181
PAniPyPA-1.0	—	—	—	—	—	63.7	11	2.0	23.4	0.182
NC	0.5	0.2	219	733	1.3	88.1	8	0	6.8	0
NPC-0.1	0.3	0.1	166	407	1.5	86.4	8	0.4	5.3	0.050
NPC-0.2	0.3	0.1	148	354	1.7	86.2	7.3	0.8	5.7	0.109
NPC-0.5	0.3	0.1	169	297	1.8	82.2	6.2	2.1	9.5	0.338
NPC-1.0	0.2	0.02	133	182	2.3	79.7	7	2.8	10.5	0.400

① Total pore volume determined from the amount of N_2 adsorbed at $p/p_0 = 0.97$.
② Micropore volume and mesopore surface area estimated by t-plot method.
③ Specific surface area calculated by BET method.
④ Pore radius estimated by BJH method.
⑤ Elemental concentration derived from XPS analysis.

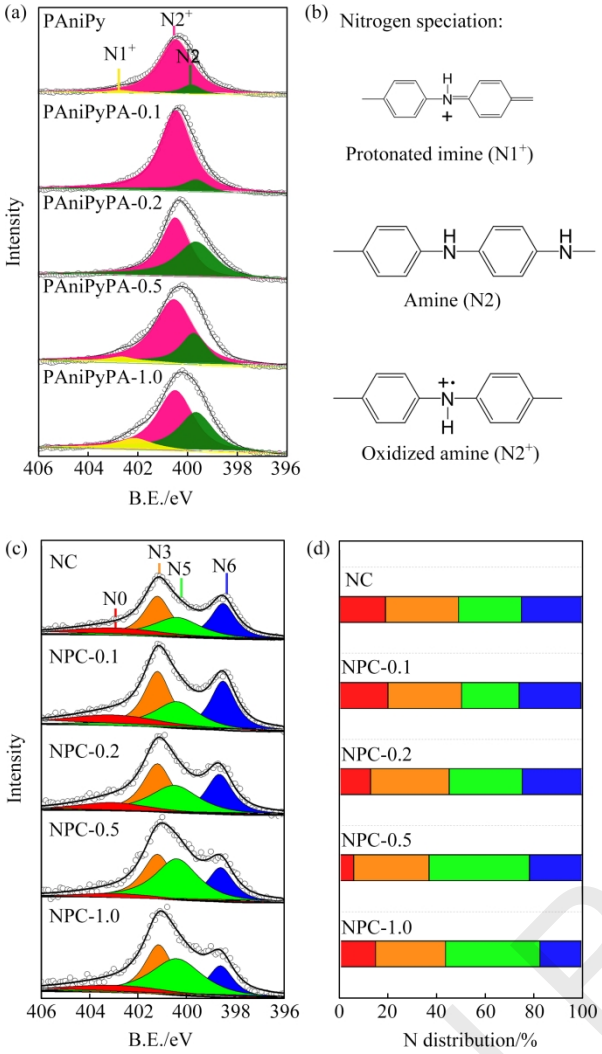

Fig. 3. N 1*s* XPS spectra of (a) PAniPy and PAniPyPA-*x* and (c) NC and NPC-*x*, accompanied with (b) the illustrations of different nitrogen speciation in the polymers, and (d) the distribution of N species in different nanocarbons. Raw data in a,c were presented in circles, and the fitted spectra were showed as the black lines.

3.1.3. Morphological evolution

The morphologies of the obtained PAniPyPA-*x* were examined by SEM (Figs. 4(a)−(d)). The benchmark PAniPy exhibited homogeneous nanosphere morphology with a diameter of about 150−170 nm. The ternary assemblies also exhibited nanosphere morphologies, but probably with a much denser structure. Accordingly, the diameters of the nanospheres slightly reduced to about 120 and 100 nm, respectively, for PAniPyPA-0.1 and PAniPyPA-0.2 (Fig. S1). With further increasing the P:N ratio, the nanosphere morphology disappeared and more 3D segregates with

cauliflower-like morphology, which was similar to those of the polyaniline-based polymers[32, 38], were found for PAniPyPA-0.5 and PAniPyPA-1.0. Noted that the sizes of these assemblies were much smaller for the latter, implying a denser structure of ternary copolymer with enriched phosphorous species. The corresponding TEM images of the PAniPyPA-*x* were recorded (Figs. 4(e) −(h)). In line with the SEM observations, hollow nanospheres were visualized for the ternary copolymers at $x \leq 0.2$, while both the hollow structures and the nanosphere morphologies were altered at higher P:N ratios. Altogether, these results clearly demonstrated the gradual fragmentation of the hollow nanosphere structures upon increasing concentration of phytic acid in the copolymerization solution. the copolymerization was supposed to occur at the interface of the micelle. The previous study [31] suggested that the copolymerization of aniline and pyrrole in the presence of the surfactant occurs at the interface of the micelle. In this case, the monomers will stay inside the space of the micelle, while the oxidant – ammonium persulfate is water soluble and would thus stay in the water phase. However, this process might be jeopardized by the participation of an additional monomer-phytic acid since it is also water soluble. Thus, with the increasing concentration of phytic acid, the hollow structure would change into more and more irregular shapes.

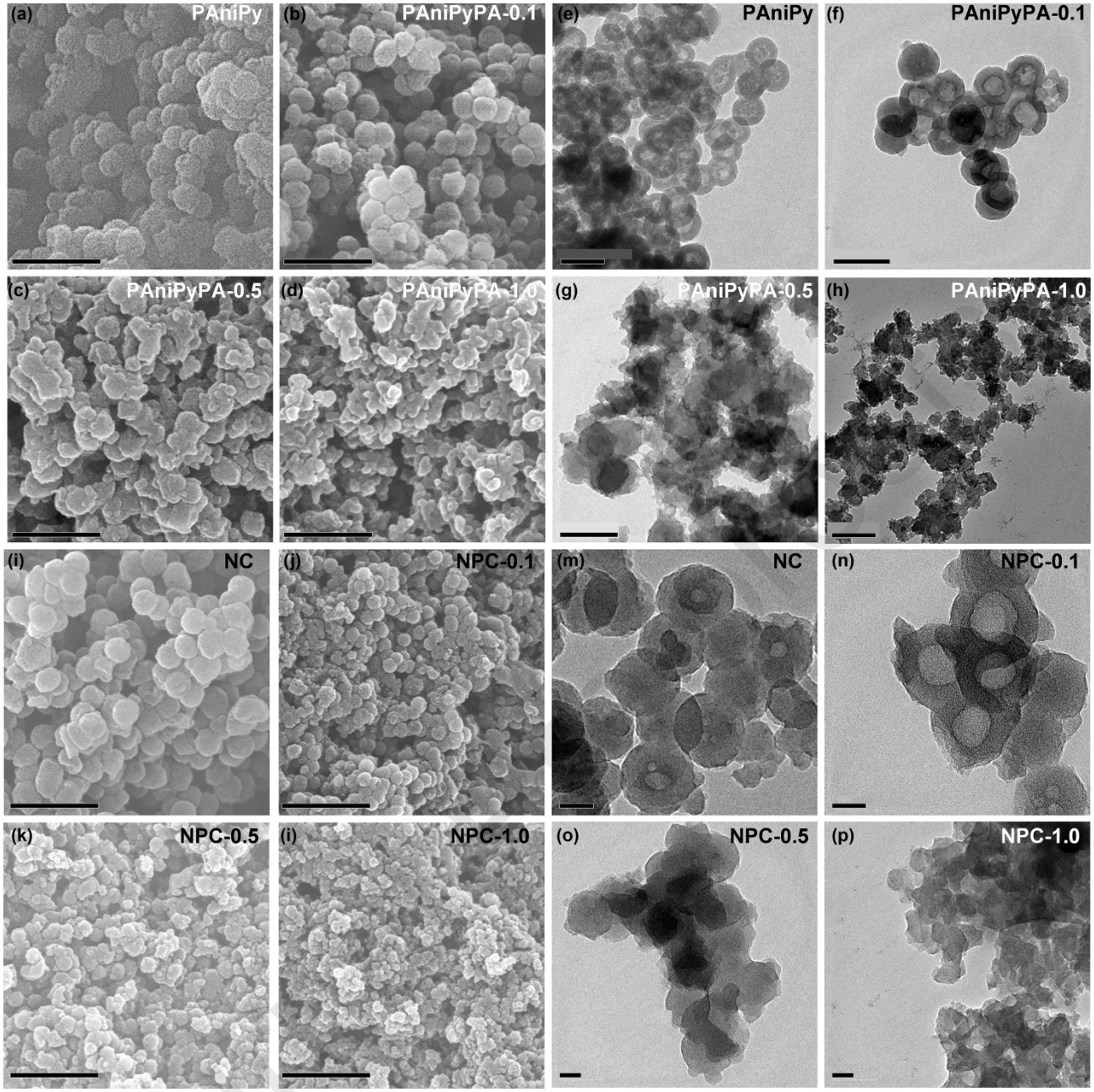

Fig. 4. (a-d, i-l) SEM and (e-h,m-p) TEM images of PAniPy and PAniPyPA-*x* polymers and corresponding NC and NPC-*x*. *x* = 0.1, 0.5, and 1.0. Scale bars: (a-d, i-l) 500 nm, and (e-h,m-p) 200 nm.

3.2. Characterization of N- and P-doped nanocarbons

3.2.1. Morphological and structural examination

The morphologies of NPC-*x* were examined by SEM and TEM (Figs. 4(i)−(p) and S1). In general, the different NPCs resembled their corresponding copolymers in morphology, which was frequently

observed in the polyaniline-derived nitrogen-doped carbons[32, 33, 39]. Different from the previous studies, we found the hollow nanostructures of PAniPy/PAniPyPA-*x* cannot be fully preserved in NC/NPC-*x*. Particularly, the hollow structures disappeared totally at $x \geq 0.2$. It was speculated that a shrinkage of the size might occur due to the high-temperature annealing treatment. To support this conclusion, we compared the diameters of nanospheres between NC or NPC-*x* and their precursors. Indeed, the diameters of carbon nanospheres were generally smaller than their individual precursors, for example, *ca*. 100 *vs*. 160 nm for NC, and *ca*. 110 *vs*. 120 nm for NPC-0.1. A closer look at the SEM images (Fig. S1) of the copolymers before and after pyrolysis revealed the presence of abundant micropores on NPC-*x* likely due to the release of exhausted gases during heat treatment. The porosity of NPC-*x* was further evaluated by N_2 sorption isotherm (Fig. 5(a)). NC possessed the highest specific surface area and the total volume (Table 1). The rich micropores and abundant mesopores were evidenced by the steep N_2 uptake at the low P/P_0 and the presence of a hysteresis loop in the sorption isotherm. With the increasing P:N ratios, the average pore size increased, while both the specific surface area and the total pore volume showed an opposing trend (Fig. 5(b)). In particular, the losses were much severer at $x<0.1$ and $x>0.5$. Therefore, these results also confirmed the aggregation of NPC-*x* with enriched P doping, agreeing well with the microscopic analysis.

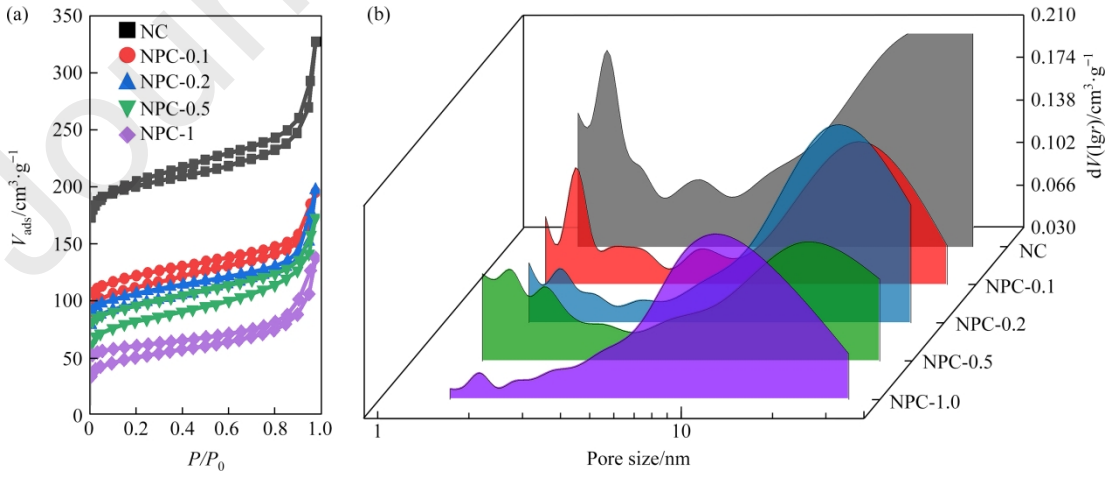

Fig. 5. (a) N_2 sorption isotherms and (b) pore size distribution of NC and NPC-*x* samples.

3.2.2. Elemental and speciation analysis from XPS

The elemental and speciation analysis of the functionalized carbons derived from the pyrolysis of the copolymers were conducted based on XPS and the results were presented in Table 1. Elemental analysis of the surface atoms revealed relatively consistent concentrations of N (6.2%−8.0% (atom)) for NPC-*x*, and the values were more apparently reduced for those samples with higher P doing levels as compared to NC. In addition, NPC-*x* showed much lower N contents than the corresponding precursors (10.5%−12.6% (atom) N). In stark contrast, the P concentrations were quite comparable for these samples before and after pyrolysis. As a result, a higher molar P:N ratio was found for all the copolymers after carbonization treatment. The above observations also suggested a higher stability of the P species than the N species in the copolymer backbone structures. For the NPC-*x* series, the O content increased with the increasing P doping, particular for the samples with higher P concentrations ($x > 0.5$). The similar trends for the P and O concentrations might indicate the presence of phosphate groups in NPC-*x*. This was supported by the presence of an envelope around 133.1 eV for the P 2*p* XPS on all the NPC-*x* samples (Fig. S2). Since alteration of the nitrogen speciation was previously evidenced for the PAniPyPA-*x* series, we further compared the N 1*s* XPS spectra of the corresponding NPC-*x* (Fig. 3(c), (d)). A broad envelop at 396−404 eV with apparent shoulder peaks were found for all the samples. To better differentiate the different nitrogen functionalities, a detailed spectra fitting was conducted (Table S1). It is found that at $x > 0.5$, the share of pyrrolic N was generally higher, but the share of pyridinic N showed a different trend, while the share of graphitic N was not quite altered in the whole series. Therefore, the incorporation of P might favor the formation of pyrrolic N speciation.

3.3. Electrochemical performance

The developed NPC-*x* series were employed as anodes for lithium ion batteries to examine the

impact of P doping on the electrochemical performance. The four-probe measurement on the electronic conductivity revealed little difference between NC and NPC-*x* (Fig. S3). We first tested NPC-0.5 electrodes in the voltage range of 0.01-3.0 V versus Li^+/Li (Fig. S4a). Typical cathodic peaks were observed at 0.6−0.9 V in the first discharge cycle that can be associated with the formation of solid electrolyte interphase[40]. This feature disappeared in the next two cycles, hinting the good reversibility of NPC-0.5 as anode for lithium ion batteries. A comparison on the capacities of NPC-*x* at 0.1 $A \cdot g^{-1}$ was presented in Fig. 6(a). The capacities were 668, 724, and 763 $mA \cdot h \cdot g^{-1}$, respectively, for NPC-0.1, NPC-0.5, and NPC-1.0, and 684 $mA \cdot h \cdot g^{-1}$ for NC. This might indicate that the storage capacity can be mildly enhanced only when doping with sufficient P. Although P-doped NPC-0.1 delivered a slightly low capacity at 0.1 $A \cdot g^{-1}$, even little lower than that of NC, it showed superior capacity of 252 $mA \cdot h \cdot g^{-1}$ at a high current density of 5 $A \cdot g^{-1}$, exceeding that of NC (219 $mA \cdot h \cdot g^{-1}$). Therefore, the results clearly displayed that the rate capability of as-prepared nanocarbons could be improved while introducing P heteroatoms. Remarkably, NPC-0.5 showed the highest capacity of 288 $mA \cdot h \cdot g^{-1}$ at 5 $A \cdot g^{-1}$ among the NPC-*x* series (Fig. 6(b), Fig. S4b), and is comparable to the previously reported hollow carbon nanospheres with rich N contents[32]. When switching the current density back to 0.1 $A \cdot g^{-1}$, a relatively high capacity of NPC-0.5 with 553 $mA \cdot h \cdot g^{-1}$ could still be obtained. The excellent rate performance was attributed to the fast charge transfer kinetics of NPC-0.5 with the lowest semicircle (R_{ct} = 22 Ω) in the high frequency region of EIS spectra (Fig. 6(c)). In addition, the cycling performance of the selected samples was further examined in the continued 200 cycles at 2 $A \cdot g^{-1}$ (Fig. 6(d)). Outstanding current efficiency of > 99.8% was obtained over all the samples. NPC-0.5 could deliver a reversible capacity of 380 $mA \cdot h \cdot g^{-1}$, which was higher than those of NC (308 $mA \cdot h \cdot g^{-1}$) and NPC-1.0 (345 $mA \cdot h \cdot g^{-1}$). A significant capacity drop for the first few cycles was observed for NPC-0.5, which might be tentatively ascribed to the lower negative electrode potential *vs*. lithium (Li/Li^+), to the formation of solid electrolyte interphase, or the loss of N and P dopants during the lithium

intercalation into the host. More importantly, NPC-0.5 exhibited superior stability to NPC-1.0 that suffered fast loss of capacity after 80 cycles.

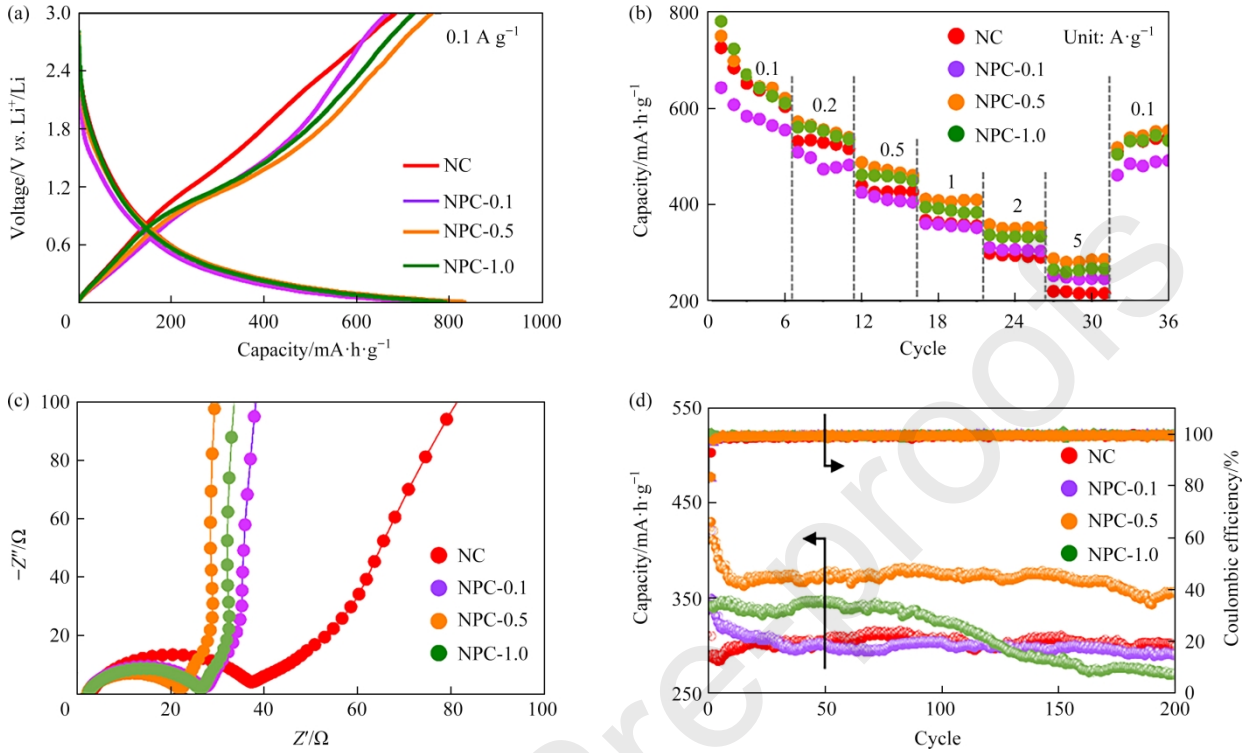

Fig. 6. Electrochemical performance of NC and NPC-*x* as anodes for lithium ion batteries in $LiPF_6$ electrolyte in the potential of 0.01 to 3.0 V versus Li^+/Li. (a) GCD profiles measured at 0.1 $A \cdot g^{-1}$. (b) Rate capability recorded at different current densities from 0.1 to 5 $A \cdot g^{-1}$. (c) EIS plots. (d) Cycling performance tested at 2 $A \cdot g^{-1}$. For the convenience of comparison, the initial Coulombic efficiency was reported in Fig. S5.

To explain the improved electrochemical performance of NPC-0.5, we first looked at the electronic conductivity. It turns out that all the materials possess similar electronic conductivity (Fig. S5). We then examined the total N contents and the different functionalities. Since the total nitrogen was relatively stable and in fact the best performing sample had the lowest N content, thus the role of this feature could be excluded. Turning to the different nitrogen functionalities, one can only find a generally positive correlation of the capacity as a function of the N5 speciation (Fig. 7, light blue symbols), however, a drop in capacity was observed for NPC-1.0 that possessed an even higher surface N5 concentration. A Similar trend was evidenced between the capacity and the surface P

concentration or the S_{BET} (Fig. 7, blue and purple symbols). Putting all these factors into account, one could find the NPC-0.5 sample showed the most balanced N5 and P concentrations as well as a relatively high S_{BET}. Therefore, it is concluded that the superior performance is originated from the rich porosity that might facilitate the mass transfer, and the large number of active species for lithium-ion storage.

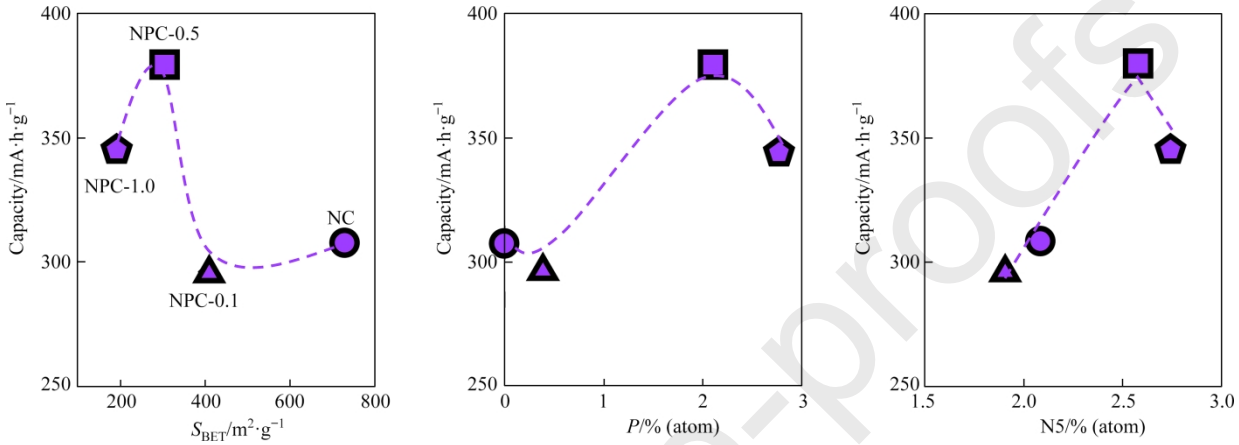

Fig. 7. Electrochemical performance as a function of the specific surface area (left), the surface concentrations of *P* content (middle) and N5 species (right).

4. Conclusions

We have developed a novel approach to synthesize a range of N- and P-doped nanocarbons with relatively consistent N dopant (6.2%−8.0% (atom) N) and varying P concentrations (0.4%−2.8% (atom) P) by the assembly of different monomers (aniline, pyrrole, and phytic acid) following subsequent pyrolysis. We studied the detailed compositional, structural, and morphological evolution of these new polymers and the nanocarbon analogues by tuning the molar P:N ratios in the starting monomers. Several key conclusions were derived: *i*) the fragmentation of hollow polymer nanospheres was evidenced with the increasing addition of phytic acid, revealing the competing polymerization between aniline-pyrrole and the aniline/pyrrole-phytic acid; this led to

novel N- and P-bearing hollow nanospheres and dense aggregates at low and high phosphorous doping levels, respectively; and *ii*) the assembly of phytic acid in the ternary polymerization system was self-limiting, reaching a plateau at around P:N = 0.5; conversely, the specific surface area and the porosity showed a trade-off with the increased P doping concentrations. Electrochemical performance of the series of derived NPC-*x* in lithium-ion batteries demonstrated their superiority over the NC counterpart. In particular, the NPC-0.5 possessing relatively high P and pyrrolic N concentrations and rich porosity exhibited the best electrochemical activity and stability performance over the other analogues, revealing the importance of balancing both factors in improving the electrochemical performance. Our work paves a new avenue for the design of high-capacity metal-free anodes for lithium ion batteries.

Acknowledgements

We thank the financial support from Zhejiang Normal University (YS304320035, YS304320036), the National Key R@D Program of China (2016YFB0100100, 2016YFA0200200), the National Natural Science Foundation of China (51872283, 22075279, 21805273, 22005297, 22005298), the Liao Ning Revitalization Talents Program (XLYC1807153), the Central Government of Liaoning Province Guides the Funds for Local Science and Technology Development (Grant 2021JH6/10500112), Dalian Innovation Support Plan for High Level Talents (2019RT09), Dalian National Laboratory For Clean Energy (DNL), CAS, DNL Cooperation Fund, CAS (DNL201912, DNL201915), DICP (DICP ZZBS201708, DICP ZZBS201802, DICP I2020032).

References（需要添加每篇文献的文章题目）

[1] X. Liu, L. Dai, Carbon-based metal-free catalysts, *Nat. Rev. Mater.*(1) (2016) 16064.https://www.nature.com/articles/natrevmats201664\">

[2] D.S. Su, G.D. Wen, S.C. Wu, F. Peng, R. Schlögl, Carbocatalysis in liquid-phase reactions, *Angew. Chem. Int. Ed.* 56 (4) (2017) 936–964.https://doi.org/10.1002/anie.201600906

[3] Z.H. Zhao, M.T. Li, L.P. Zhang, L.M. Dai, Z.H. Xia, Design principles for heteroatom-doped carbon nanomaterials as highly efficient catalysts for fuel cells and metal-air batteries, *Adv. Mater.* 27 (43) (2015) 6834–6840.https://pubmed.ncbi.nlm.nih.gov/26418520/

[4] Z.H. Wang, X. Feng, Y. Bai, H.Y. Yang, R.Q. Dong, X.R. Wang, H.J. Xu, Q.Y. Wang, H. Li, H.C. Gao, C. Wu, Probing the energy storage mechanism of quasi-metallic Na in hard carbon for sodium-ion batteries, *Adv. Energy Mater.* 11 (11) (2021) 2003854.https://doi.org/10.1002/aenm.202003854

[5] B.H. Hou, Y.Y. Wang, Q.L. Ning, W.H. Li, X.T. Xi, X. Yang, H.J. Liang, X. Feng, X.L. Wu, Sodium-ion batteries: self-supporting, flexible, additive-free, and scalable hard carbon paper self-interwoven by 1D microbelts: superb room/low-temperature sodium storage and working mechanism (adv. mater. 40/2019), *Adv. Mater.* 31 (40) (2019) 1970288.https://doi.org/10.1002/adma.201970288

[6] H.J. Liang, Z.Y. Gu, X.Y. Zheng, W.H. Li, L.Y. Zhu, Z.H. Sun, Y.F. Meng, H.Y. Yu, X.K. Hou, X.L. Wu, Tempura-like carbon/carbon composite as advanced anode materials for K-ion batteries, *J. Energy Chem.* 59 (2021) 589–598.http://dx.doi.org/10.1016/j.jechem.2020.11.039

[7] G. Wang, X.H. Xiong, D. Xie, Z.H. Lin, J. Zheng, F.H. Zheng, Y.P. Li, Y.Z. Liu, C.H. Yang, M.L. Liu, Chemically activated hollow carbon nanospheres as a high-performance anode material for potassium ion batteries, *J. Mater. Chem. A* 6 (47) (2018) 24317–24323.https://doi.org/10.1039/c8ta09751h

[8] C.L. Ma, Z.H. Hu, N.J. Song, Y. Zhao, Y.Z. Liu, H.Q. Wang, Constructing mild expanded graphite microspheres by pressurized oxidation combined microwave treatment for enhanced lithium storage, *Rare Met.* 40 (4) (2021) 837–847.http://dx.doi.org/10.1007/s12598-020-01625-9

[9] M.N. Fan, Z.H. Lin, P. Zhang, X.D. Ma, K.P. Wu, M.L. Liu, X.H. Xiong, Synergistic effect of nitrogen and sulfur dual-doping endows TiO_2 with exceptional sodium storage performance, *Adv. Energy Mater.* 11 (6) (2021) 2003037.https://doi.org/10.1002/aenm.202003037

[10] K.P. Gong, F. Du, Z.H. Xia, M. Durstock, L.M. Dai, Nitrogen-doped carbon nanotube arrays with high electrocatalytic activity for oxygen reduction, *Science* 323 (5915) (2009) 760–764.https://pubmed.ncbi.nlm.nih.gov/19197058/

[11] M. Borghei, N. Laocharoen, E. Kibena-Põldsepp, L.S. Johansson, J. Campbell, E. Kauppinen, K. Tammeveski, O.J. Rojas, Porous N, P-doped carbon from coconut shells with high electrocatalytic activity for oxygen reduction: alternative to Pt-C for alkaline fuel cells, *Appl. Catal. B Environ.* 204 (2017) 394–402.http://dx.doi.org/10.1016/j.apcatb.2016.11.029

[12] X.S. Dong, X.W. Liu, H. Chen, X.Y. Xu, H.C. Jiang, C.L. Gu, Q. Li, S.L. Qiao, X.J. Zhang, Y.Q. Hu, Hard template-assisted N, P-doped multifunctional mesoporous carbon for supercapacitors and hydrogen evolution reaction, *J. Mater. Sci.* 56 (3) (2021) 2385–2398.http://dx.doi.org/10.1007/s10853-020-05303-0

[13] J. Gao, N. Ma, J.J. Tian, C. Shen, L.L. Wang, P.F. Yu, Y.Y. Chu, W. Liu, X.Y. Tan, X.F. Li, Z. Yin, High performance of N, P co-doped metal-free carbon catalyst derived from ionic liquid for oxygen reduction reaction, *J. Solid State Electrochem.* 22 (2) (2018) 519–525.http://dx.doi.org/10.1007/s10008-017-3785-y

[14] R. Li, Z.D. Wei, X.L. Gou, Nitrogen and phosphorus dual-doped graphene/carbon nanosheets as bifunctional electrocatalysts for oxygen reduction and evolution, *ACS Catal.* 5 (7) (2015) 4133–4142.https://doi.org/10.1021/acscatal.5b00601

[15] T.H. Li, D.M. Tang, M. Wang, Q.L. Song, C.M. Li, Ionic liquid originated synthesis of N, P-doped graphene for hydrogen evolution reaction, *ChemistrySelect* 3 (24) (2018) 6814–6820.https://doi.org/10.1002/slct.201801439

[16] Y.N. Sun, M.L. Zhang, L. Zhao, Z.Y. Sui, Z.Y. Sun, B.H. Han, A N, P dual-doped carbon with high porosity as an advanced metal-free oxygen reduction catalyst, *Adv. Mater. Interfaces* 6 (14) (2019) 1900592.https://doi.org/10.1002/admi.201900592

[17] Z. Zhou, A. Chen, X. Fan, A. Kong, Y. Shan, Hierarchical porous N-P-coupled carbons as metal-free bifunctional electro-catalysts for oxygen conversion, *Appl. Surf. Sci.* 464 (2019) 380–387.http://dx.doi.org/10.1016/j.apsusc.2018.09.095

[18] S. Kar, K. Bramhaiah, N.S. John, S. Bhattacharyya, Insight into the multistate emissive N, P-doped carbon nano-Onions: emerging visible-light absorption for photocatalysis, *Chem. Asian J.* 16 (9) (2021) 1138–1149.https://pubmed.ncbi.nlm.nih.gov/33734603/

[19] Q.M. Sun, Y.M. Li, T. He, The excellent capacitive capability for N, P-doped carbon microsphere/reduced graphene oxide nanocomposites in H_2SO_4/KI redox electrolyte, *J. Mater. Sci.* 54 (10) (2019) 7665–7678.http://dx.doi.org/10.1007/s10853-019-03414-x

[20] W. Zhong, Q.W. Chen, F. Yang, W.L. Liu, G.D. Li, K.F. Xie, M.M. Ren, N, P dual-doped carbon nanotube with superior high-rate sodium storage performance for sodium ion batteries, *J. Electroanal. Chem.* 850 (2019) 113392.http://dx.doi.org/10.1016/j.jelechem.2019.113392

[21] G.H. Dong, K. Lang, H. Ouyang, W.Z. Zhang, L.M. Bai, S.J. Chen, Z.F. Zhang, Y.Y. Gao, Z.H. Mu, X.D. Zhao, Facile synthesis of N, P-doped carbon dots from maize starch *via* a solvothermal approach for the highly sensitive detection of Fe^{3+}, *RSC Adv*. 10 (55) (2020) 33483–33489.https://doi.org/10.1039/d0ra06209j

[22] J.J. Li, Y.Z. Jiao, L.D. Feng, Y. Zhong, G.C. Zuo, A.M. Xie, W. Dong, Highly N, P-doped carbon dots: rational design, photoluminescence and cellular imaging, *Microchimica Acta* 184 (8) (2017) 2933–2940.http://dx.doi.org/10.1007/s00604-017-2314-0

[23] Y.J. Gao, G. Hu, J. Zhong, Z.J. Shi, Y.S. Zhu, D.S. Su, J.G. Wang, X.H. Bao, D. Ma, Nitrogen-doped sp^2-hybridized carbon as a superior catalyst for selective oxidation, *Angew. Chem. Int. Ed.* 52 (7) (2013) 2109–2113.https://doi.org/10.1002/anie.201207918

[24] D.H. Guo, R. Shibuya, C. Akiba, S. Saji, T. Kondo, J. Nakamura, Active sites of nitrogen-doped carbon materials for oxygen reduction reaction clarified using model catalysts, *Science* 351 (6271) (2016) 361–365.https://pubmed.ncbi.nlm.nih.gov/26798009/

[25] L. He, F. Weniger, H. Neumann, M. Beller, Synthesis, characterization, and application of metal nanoparticles supported on nitrogen-doped carbon: catalysis beyond electrochemistry, *Angewandte Chemie Int. Ed.* 55 (41) (2016) 12582–12594.http://dx.doi.org/10.1002/anie.201603198

[26] J. Yang, M. Xu, J.Y. Wang, S.B. Jin, B.E. Tan, A facile approach to prepare multiple heteroatom-doped carbon materials from imine-linked porous organic polymers, *Sci. Rep.* 8 (1) (2018) 4200.https://pubmed.ncbi.nlm.nih.gov/29523847/

[27] Y.L. Xia, Z.Z. Zhang, F.X. Qin, J. Gao, H. Wang, Z.W. Xu, X.Y. Tan, X. Liu, X.F. Li, Z. Yin, Electrocatalytic activity enhancement of N, P-doped carbon nanosheets derived from polymerizable ionic liquids, *J. Appl. Electrochem.* 51 (4) (2021) 669–679.http://dx.doi.org/10.1007/s10800-020-01506-0

[28] J.W.F. To, Z. Chen, H.B. Yao, J.J. He, K. Kim, H.H. Chou, L.J. Pan, J. Wilcox, Y. Cui, Z.N. Bao, Ultrahigh surface area three-dimensional porous graphitic carbon from conjugated polymeric molecular framework, *ACS Cent. Sci.* 1 (2) (2015) 68–76.https://pubmed.ncbi.nlm.nih.gov/27162953/

[29] J. Zhang, Z. Zhao, Z. Xia, L. Dai, A metal-free bifunctional electrocatalyst for oxygen reduction and oxygen evolution reactions, *Nat. Nanotechnology,*10 (5) (2015) 444–452.https://www.nature.com/articles/nnano.2015.48\">

[30] X.X. Mao, Z.X. Cao, S.N. Chen, J.Y. Jia, X.N. Li, Y.H. Yin, S.T. Yang, Facile synthesis of N, P-doped hierarchical porous carbon framework catalysts based on gelatin/phytic acid supermolecules for electrocatalytic oxygen reduction, *Int. J. Hydrog. Energy* 44 (12) (2019) 5890–5898.http://dx.doi.org/10.1016/j.ijhydene.2019.01.044

[31] C.Q. Zhou, J. Han, G.P. Song, R. Guo, Fabrication of poly(aniline-co-pyrrole) hollow nanospheres with triton X-100 micelles as templates, *J. Polym. Sci. A Polym. Chem.* 46 (11) (2008) 3563–3572.https://doi.org/10.1002/pola.22695

[32] X.L. Mou, J.X. Ma, S.H. Zheng, X.K. Chen, F. Krumeich, R. Hauert, R.H. Lin, Z.S. Wu, Y.J. Ding, A general synthetic strategy toward highly doped pyridinic nitrogen-rich carbons, *Adv. Funct. Mater.* 31 (3) (2021) 2006076.https://doi.org/10.1002/adfm.202006076

[33] F. Xu, B.C. Ding, Y.Q. Qiu, R.H. Dong, W.Q. Zhuang, X.S. Xu, H.J. Han, J.Y. Yang, B.Q. Wei, H.Q. Wang, S. Kaskel, Generalized domino-driven synthesis of hollow hybrid carbon spheres with ultrafine metal nitrides/oxides, *Matter* 3 (1) (2020) 246–

260.http://dx.doi.org/10.1016/j.matt.2020.05.012

[34] R.H. Lin, S.K. Kaiser, R. Hauert, J. Pérez-Ramírez, Descriptors for high-performance nitrogen-doped carbon catalysts in acetylene hydrochlorination, *ACS Catal*. 8 (2) (2018) 1114–1121.https://doi.org/10.1021/acscatal.7b03031

[35] S.K. Kaiser, R.H. Lin, F. Krumeich, O.V. Safonova, J. Pérez-Ramírez, Preserved in a shell: high-performance graphene-confined ruthenium nanoparticles in acetylene hydrochlorination, *Angew*. *Chem*. *Int*. *Ed*. 58 (35) (2019) 12297–12304.https://doi.org/10.1002/anie.201906916

[36] J. Stejskal, R.G. Gilbert, Polyaniline. Preparation of a conducting polymer(IUPAC Technical Report), *Pure Appl*. *Chem*. 74 (5) (2002) 857–867.https://doi.org/10.1351/pac200274050857

[37] M. Trchová, J. Stejskal, Polyaniline: The infrared spectroscopy of conducting polymer nanotubes (IUPAC Technical Report), *Pure Appl*. *Chem*. 83 (10) (2011) 1803–1817.https://doi.org/10.1351/pac-rep-10-02-01

[38] M. Trchová, P. Matějka, J. Brodinová, A. Kalendová, J. Prokeš, J. Stejskal, Structural and conductivity changes during the pyrolysis of polyaniline base, *Polym*. *Degrad*. *Stab*. 91 (1) (2006) 114–121.http://dx.doi.org/10.1016/j.polymdegradstab.2005.04.022

[39] M. Trchová, E.N. Konyushenko, J. Stejskal, J. Kovářová, G. Ćirić-Marjanović, The conversion of polyaniline nanotubes to nitrogen-containing carbon nanotubes and their comparison with multi-walled carbon nanotubes, *Polym*. *Degrad*. *Stab*. 94 (6) (2009) 929–938.http://dx.doi.org/10.1016/j.polymdegradstab.2009.03.001

[40] X.H. Liu, J. Zhang, S.J. Guo, N. Pinna, Graphene/N-doped carbon sandwiched nanosheets with ultrahigh nitrogen doping for boosting lithium-ion batteries, *J*. *Mater*. *Chem*. *A* 4 (4) (2016) 1423–1431.https://doi.org/10.1039/c5ta09066k

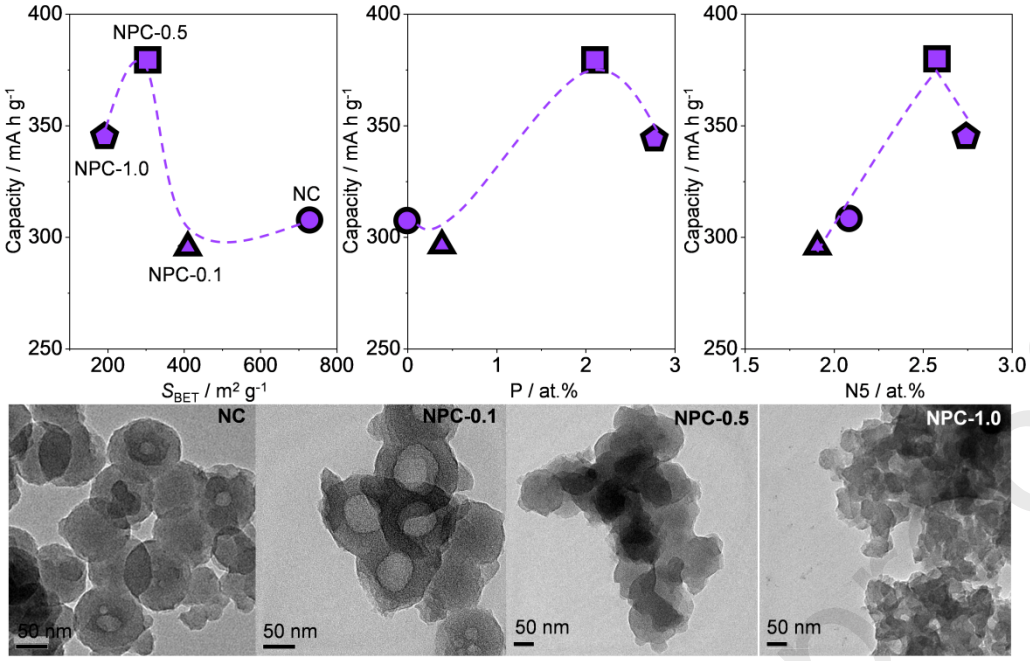

Declaration of interests

☒ The authors declare that they have no known competing financial interests or personal relationships that could have appeared to influence the work reported in this paper.

☐The authors declare the following financial interests/personal relationships which may be considered as potential competing interests: